Numerical Study of Blade-Vortex Interaction (BVI) Noise Capturing

Yasutada Tanabe* and Shigeru Saito*
Aviation Program Group, Japan Aerospace Exploration Agency (JAXA)
7/44-1 Jindaiji Higashi-machi, Chofu-shi, Tokyo 182-8522, Japan

Keisuke Takasaki**
Graduate School of Science and Technology, Nihon University, Tokyo, Japan

Hajime Fujita***
Research Institute of Science, Nihon University, Tokyo, Japan

Abstract

The noise is one of the serious problems concerning helicopters operations. The issue of helicopter external noise generated mainly from a helicopter rotor has always affected the use of rotorcrafts, especially in the urban environment. The noise sources depend on the flight configurations. In particular, a noise generated by the interaction between blades and tip vortices mainly occurs during descent flight. This noise is called blade-vortex interaction (BVI) noise, and this BVI noise is particularly penalizing for helicopters. In this paper, a numerical study to capture the BVI noise is carried out. The numerical study is performed in two phases. In the first phase, a 2D simulation based on parallel BVI event of Kitapliglu et al experiment is performed. In the second phase, 3D simulation based on HART II experiment is performed. Several experimental data such as thrust, torque, blade sectional load, its derivative and vortex location are compared with calculation results and the comparison showed reasonably good agreement.

Key words : JAXA, Blade-Vortex Interaction(BVI), Noise, Helicopter Rotor,
         HART II

Introduction

The Blade-Vortex Interaction (BVI) is the main cause of the annoying noise and vibration for helicopter especially during the descending flight. The strongest part of this BVI phenomenon occurs while the blade strikes on or passes closely the tip vortices shed from preceding blades. Accurate capturing of BVI numerically is important to understand the mechanism of BVI phenomena and vital to evaluate the capabilities of rotor noise reduction devices and other noise abatement flight procedures. It remains as a challenging subject for rotorcraft researchers mostly because of the difficulties to preserve the tip vortex wakes.

* Senior Researcher
** Graduate Student
*** Professor
   E-mail : tan@chofu.jaxa.jp   Tel : +81-422-40-3230   Fax : +81-422-40-3235

There are many experiments and numerical simulations on the BVI event till now. The representative 2D BVI experiment was carried out by Kitaplioglu et al. [1, 2], and it became a good test case for comparison with CFD simulations. In their experiment, a rotor blade with zero incidence strikes with a straight line vortex generated by an independent vortex generator located in the upstream. On the other hand, a representative 3D BVI experiment was carried out in HART II project [3, 4]. This experiment is performed as an international rotor noise reduction project, and it became a good test case to evaluate the CFD simulations. Numerical simulations of the BVI have been carried out by several researchers [5−7] with certain success to capture the main features. No researches on the BVI with incident airfoil are reported at this point for the 2D case except some attempts by present authors [8].

For the simulation of the 2D event, a vortex is initially put at a far upstream location and then passes through the blade airfoil vicinity. And, for the simulation of the 3D BVI event, the phenomenon is calculated as an isolated rotor without the fuselage. Overlapped grid approach [9] is utilized for the numerical simulation. In this approach, a Cartesian background grid is used to cover a wide range of computation area (called outer background grid) and another Cartesian background grid is located around the rotor to preserve the tip vortices wake (called inner background grid). The airfoil vicinity is surrounded by a body fitted curvilinear grid (called inner moving grid or airfoil grid for short). As the numerical dissipation of the vortex has been a key problem relating with the BVI simulation, a CFD scheme with high spatial accuracy is applied to the inner and outer background grids. Combined with a moderate fine inner background grid mesh size, the initial vortex is well preserved along a long distance of convection that ensures the overall accuracy of the simulation in the 2D cases [3].

Test case

In 2D BVI event, a basic test case is selected based on the experiment by Kitaplioglu et al. [1, 2] where a parallel BVI is studied. Because the relative speed at each rotor radius position with regard to the vortex is different, only a narrow blade azimuth angle range and a limited blade section area can be regarded as a good condition to the ideal 2D parallel BVI simulation. The computational parameters are shown in Table 1. The initial vortex strength and core radius are also determined based on the measurements. More detailed descriptions of the numerical settings can be found in reference 8.

For the simulation of the 3D BVI event, a basic test case is selected based on the HART II Baseline (BL) case. The experimental set up at HART II is shown in Fig. 1.

Table 1. Computational Parameters for 2D BVI Event

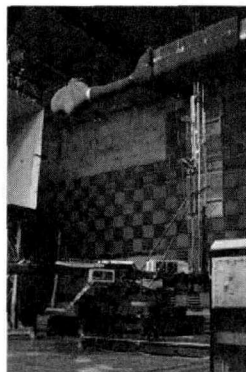| Initial miss distance Z_v [m] | 0, −0.13, −0.25, −0.4, −1.0, −1.5 |
	0.13, 0.25, 0.4, 1.0, 1.5
Airfoil incidence α [deg]	0, 2, 4, 8
Vortex rotation	Clockwise, Counter−clockwise

Fig. 1. Experimental Set−up at HART II [3, 4]

Table 2. HART II Baseline case conditions

Rotor radius	R=2m
Blade chord length	c=0.121m
Twist angle	−8.0° /rad
Precone angle	$\beta_0=2.5°$
Number of blade	NBLD=4
Free stream Mach number	$M_\infty=0.4$
Tip Mach number	$M_{tip}=0.6349$
Airfoil	Modified NACA23012
Advance ratio	0.1512
Rotor shaft angle	$\alpha_q=-4.2°$
Rotor operating speed	1041rmp
Thrust Coefficient	$C_T≈0.0044$

The rotor model is a 40% Mach scaled model of BO105 helicopter. In 1994, and then 2001, this model has been tested in the DNW wind tunnel during the HART and HART II campaigns [3, 4], whose objective was to analyze the influence of the High Harmonic Control to reduce the Blade−Vortex Interaction noise. Very complete measurements have been obtained on the rotor which was equipped with a hub allowing a multicyclic control of pitching angle. These parameters are shown in Table 2.

the present analysis, the blades are supposed to be rigid, so no elastic deformations are applied. The blade dynamics used in the CFD has been obtained from a trim analysis using a comprehensive code of Eurocopter. Multicycled flapping, lead−lagging and feathering motions are prescribed to simulate the measured blade motions [6].

Numerical Method

3.1 Overlapped grid approach

The overlapped grid approach [9] is used for this study. As shown in Fig. 2 and Fig. 3, there are three layers of computational grid. Fig. 2 is 2D grid system and, Fig. 3 is 3D grid system. A wide outer background grid with coarser grid resolution is used for preservation of the flow field boundary conditions. A fine resolution inner background grid is used to cover the path of vortex convection and preserve the initial vortex from numerical dissipation. An airfoil grid is used for the computation around the airfoil. For computational efficiency, Cartesian type grids are used for the background grids and a 4th order high resolution numerical scheme based on SHUS scheme [10] is used. For time integration, 4 stages Runge−Kutta method suggested by Jameson et al. [11] is used. The airfoil grid is curvilinear, and a 2nd order Yee−Harten TVD scheme [12] is adopted.
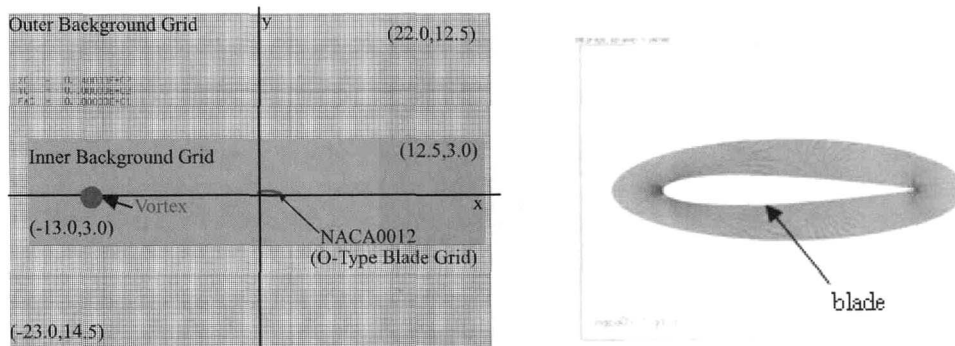
(a) Whole computational Domains   (b) Blade grid
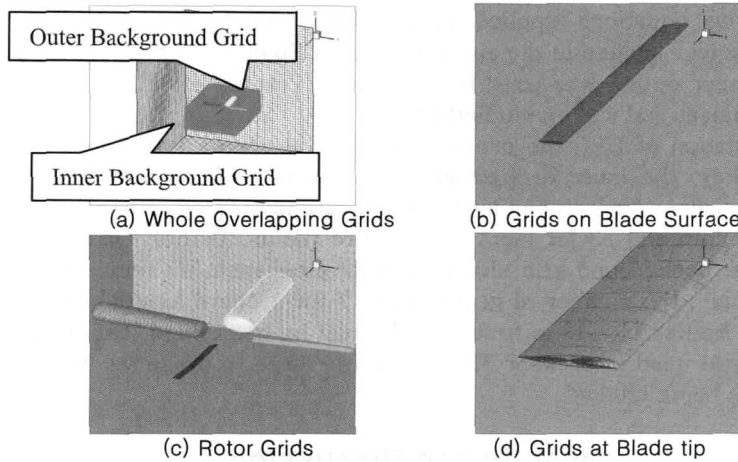Fig. 2. Moving Overlapped Grid Approach at 2D case

(a) Whole Overlapping Grids   (b) Grids on Blade Surface

(c) Rotor Grids   (d) Grids at Blade tip

Fig. 3. Moving Overlapped Grid Approach at 3D case

3.2 CFD procedural

Fig. 4. shows CFD procedure for overlapped grid approach. The computation starts from the outer background, and then computation in inner background grid is executed with the boundary values interpolated from the outer background grid. Then, with the outer boundary values obtained from the inner background grid, computation in the airfoil grid is advanced. The whole airfoil grid values are interpolated onto the overlapped area with the inner background grid. Finally, inner background grid values are interpolated onto the overlapped area with the outer background grid to finish one cycle of computation.

For present study, a common time step is pre-designated and the information is exchanged between each layer of grid at this time step. And for computation in each layer of grid, divided time steps are used to meet the each given maximum allowable CFL number. Because the numerical scheme for the background grid is an explicit one, a CFL number is given less than 0.8 in 2D computation and 0.9 in 3D computation. For the inner airfoil grid, a CFL number is given less than 25 in 2D computation and 20 in 3D computation. With such strategy, an efficient and robust simulation code is developed.
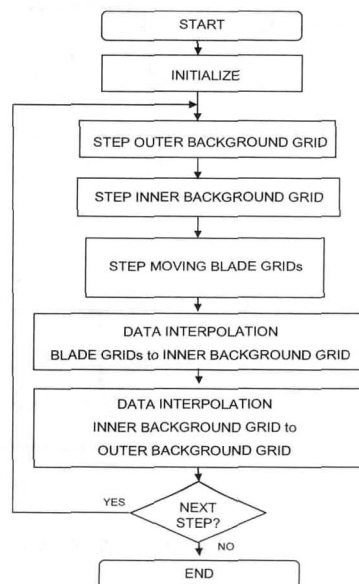

Fig. 4. CFD procedure for Overlapped Grid Approach

The governing equations applied in the background grids are Euler equations. Although the CFD solver applied in the airfoil grid is an Euler/Navier−Stokes equation solver, only the inviscid Euler option was used in this study. Viscous effect on the parallel BVI is considered not dominant and will be studied later.

For the simulation of BVI, the preservation of the vortex is the key to the accurate solution. In this study, the inner background grid size is an important factor. For 2D BVI event simulation, the inner background grid size has already tested. The number of grid point is 80 for 1 chord length and 13 for input vortex core radius (0.16c). On the other hand, for 3D BVI event, inner background grid size is adjusting because 3D simulation takes a lot of times. So in this study, the number of grid point is 7 for 1 chord length and 1 for tip vortex core size (4%c~12%c Ref [1, 2]) in first step. It must be mentioned that compared with the 2D case, the grid size used in present 3D is case too large to preserve the tip vortex. The effect of grid size is being studied.

Results and Discussion

4.1 Results and Discussion for 2D BVI Event

Figure 6 and 7 are the BVI level X_{bvi_sum} (factor X_{bvi} is introduced by Kitaplioglu et al [3, 4], shown in Fig. 5) changes with miss distances for various incident angles. The maximum BVI level becomes weaker and occurs at a negative initial miss distance instead of the zero initial miss distance when the airfoil has incident angles.

As another BVI level evaluation factor, L_{bvi} is determined from the sound pressure change following the definition by Kitaplioglu et al [3, 4] and shown in Fig. 5. The selected microphone in the near−field of the interaction is microphone #7 as defined in ref [1] (also shown in Fig. 8). As shown in Fig. 9 and Fig. 10, there seems have good correlation with the X_{bvi_sum} which based on the surface pressure changes. And the miss distance for the peak vale of L_{bvi} at 2~8 degrees also moves to negative side.
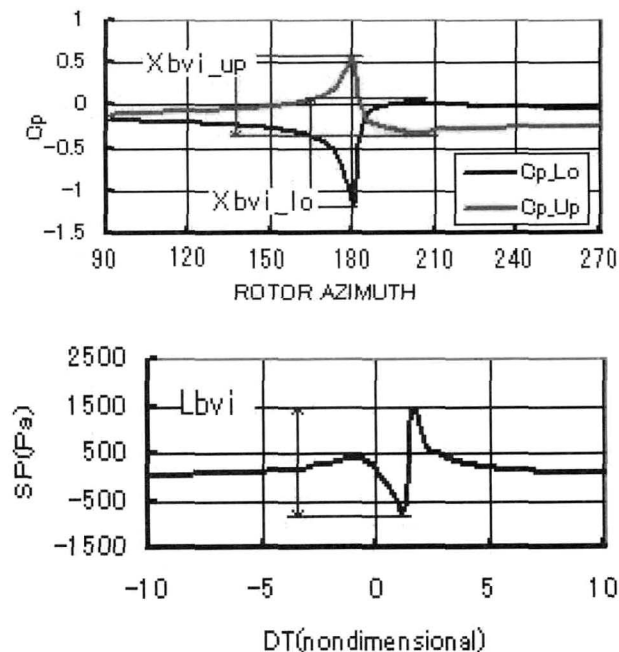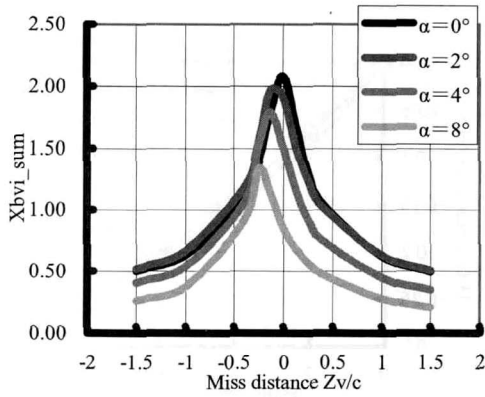

Fig. 5. Calculation of X_{bvi} and L_{bvi}

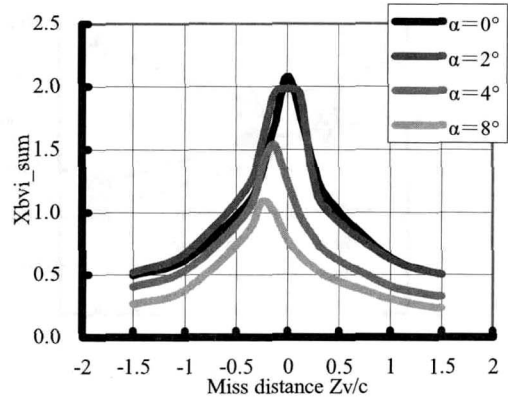Fig. 6. X_{bvi_sum} vs. initial miss distance ($\Gamma v = -0.252$)

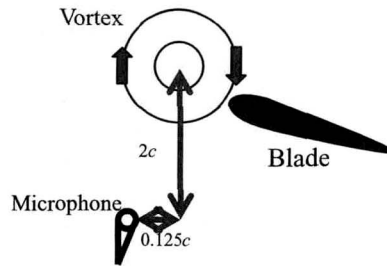Fig. 7. X_{bvi_sum} vs. initial miss distance ($\Gamma v = 0.252$)

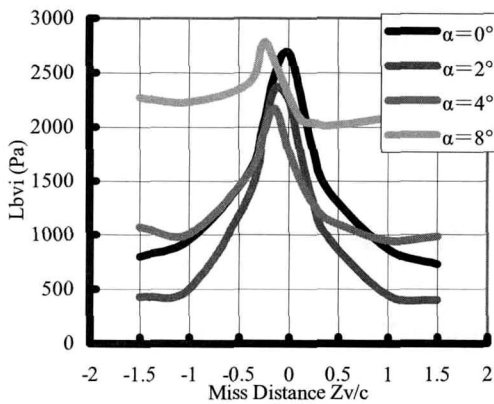Fig. 8. Near–field microphone position

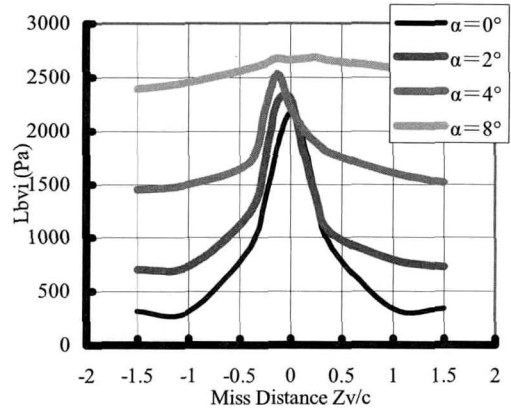Fig. 9. L_{bvi} vs. initial miss distance ($\Gamma v = -0.252$)

Fig. 10. L_{bvi} vs. initial miss distance ($\Gamma v = 0.252$)

The peak values of X_{bvi_sum} and L_{bvi} with regard to the incidence angle is shown in Fig. 11. It can be seen that the peak values of X_{bvi_sum} decrease with incidence angle both for positive and negative vortex and the peak values of L_{bvi} increase with incidence angle for positive vortex. Then for negative vortex, the peak value of L_{bvi} increase at over 4 degrees. When there is incidence angle of the airfoil, the original pressure distribution at the lower plane of the airfoil has a slow rise near the airfoil which is the source of the well–known loading noise [8].
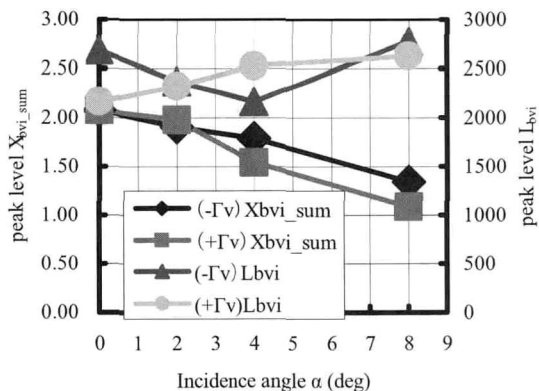
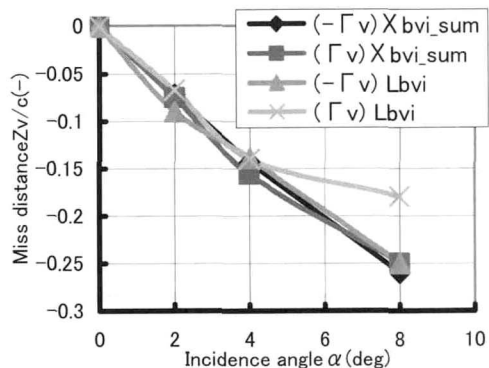Fig. 11. Peak values of X_{bvi_sum} and L_{bvi} vs airfoil incidence angle

Fig. 12. BVI level peak position vs incidence angle

As the incidence angle of the airfoil is increased, the initial miss distance of the maximum of the BVI level shift to negative side in all cases. The BVI peak locations for incident angle from 0 to 8 degrees are shown in Fig. 12. There is no difference observed in peak level position between positive and negative vortices. It can be seen the peak position shifts are nearly linearly decrease with the incidence angle of the airfoil.

The reason to cause such shifts is investigated by plotting the trajectories of the vortex while it is convected by the flow downstream. Firstly, to check if there is vertical movement of a vortex when the incidence angle is zero, the vortex trajectory is plotted in Fig. 13. It can be seen there is no noticeable vertical position change of the vortex in this case. It is concluded that there is no noticeable miss distance shift caused by the vortex itself. In Fig. 26, the airfoil incidence is 8 degrees. Fig.14 (a) is for a vortex initially located at $Zv/c=0$. As it is convected downstream, the vortex moves upward and its core center miss the airfoil leading edge. In Fig.14 (b), the vortex initially located $Zv/c=-0.25$. When it is convected by the flow, the core center of this vortex strikes the leading edge directly as a head-on interaction and causes maximum level of BVI. The upward movement of the vortex is caused by the upwash flow ahead of an airfoil with incidence angle. Also the strength of upwash is nearly proportional to the incident angle. So the relation shown in Fig.12 can be reasonably explained.
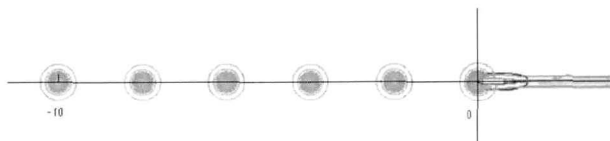

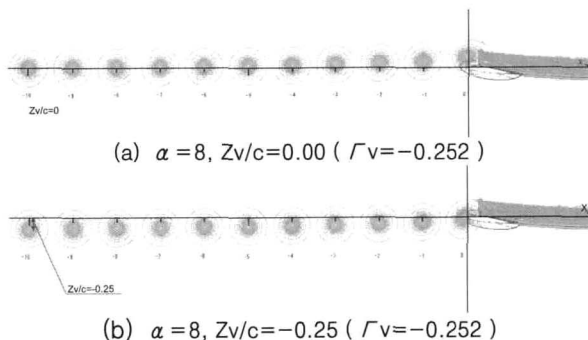Fig. 13. Vortex trajectory $\alpha =0$, $Zv/c=0.00$ ($\Gamma v=-0.252$)

(a) $\alpha =8$, $Zv/c=0.00$ ($\Gamma v=-0.252$)

(b) $\alpha =8$, $Zv/c=-0.25$ ($\Gamma v=-0.252$)

Fig. 14. Trajectories of Vortex for $\alpha =8°$

4.2 Results and Discussion for 3D BVI Event

The tip vortices are visualized with the Q-criterion iso-surfaces (also called iso-lambda2) as shown in Fig. 15. It is the rotational part of the vorticity defined by:

$$Q = -\frac{1}{2}\left(\left(\frac{\partial u}{\partial x}\right)^2 + \left(\frac{\partial v}{\partial y}\right)^2 + \left(\frac{\partial w}{\partial z}\right)^2 + 2\left(\frac{\partial u}{\partial y}\frac{\partial v}{\partial x} + \frac{\partial u}{\partial z}\frac{\partial w}{\partial x} + \frac{\partial v}{\partial z}\frac{\partial w}{\partial y}\right)\right)$$

The history of thrust coefficient C_T is shown in Fig. 16. It can be seen that the thrust is vibrating 4 times per 1 revolution because the number of blades is 4. And, the C_T vibrational amplitude is about 0.5×10^{-3}. Compared with the experiment, the averaged value is about 5% higher. Further adjustment of the prescribed blade motions might be required for better comparison with experiment.

The history of torque coefficient C_q is shown in Fig. 17. It can been seen that the torque is nearly converged to 1.5×10^{-4}.

Figure 18 and 19 show comparison between the HART II experiment and the calculation for blade airload C_nM^2 and its derivative $d(C_nM^2)/d\Psi$. Fluctuations at advancing side ($\Psi < 80°$) or at retreating side ($\Psi < 240°$) appearing both in experiment and in calculation indicate that BVI is occurring during these azimuth regions. The calculation showed much lower oscillations compared with the experiment. Using finer inner background mesh and including elastic deformation are planned as the next step.

As shown in figures 20 (a), (b) and 21 (a), (b), double cores of tip vortices are observed both at advancing side (Y=1.4) and retreating side (Y=−1.4) in the Q-criterion contour plot. Good agreement between the HART II experiment and the calculation can be observed for the upper sheets of vortices. The tip vortex is convected upwards upstream of the rotor center, and then is convected downwards in the downstream. The positions of the instantaneous vortex centers illustrate the unsteady characteristic of the wake geometry for two directions.
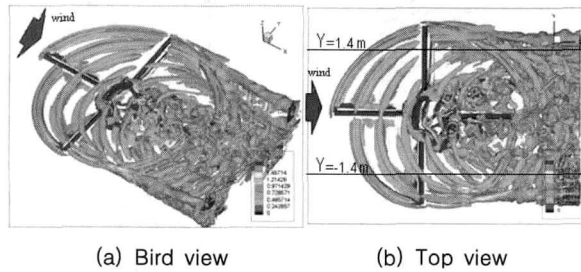

(a) Bird view   (b) Top view

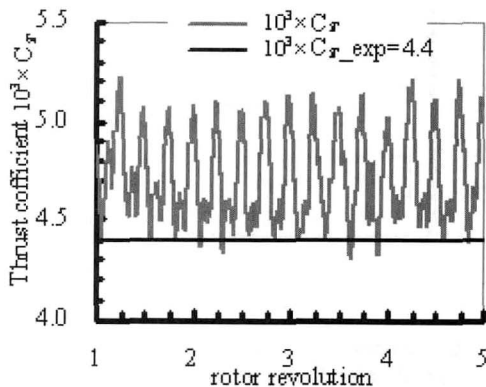Fig. 15. Iso-surface plot of Q criterion

Fig. 16. Thrust C_T history (1rev~5rev)

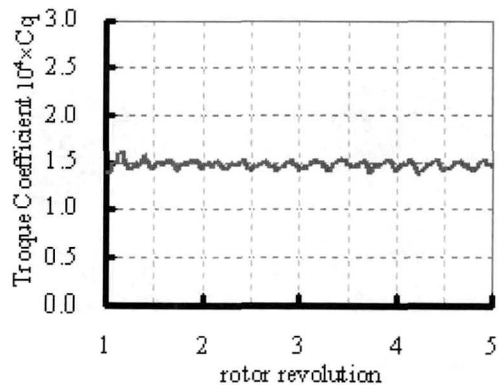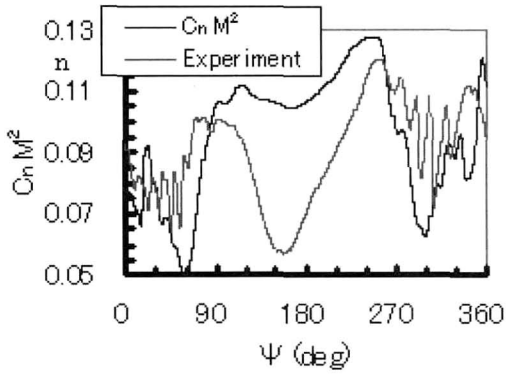Fig. 17. Torque C_q history (1rev~5rev)

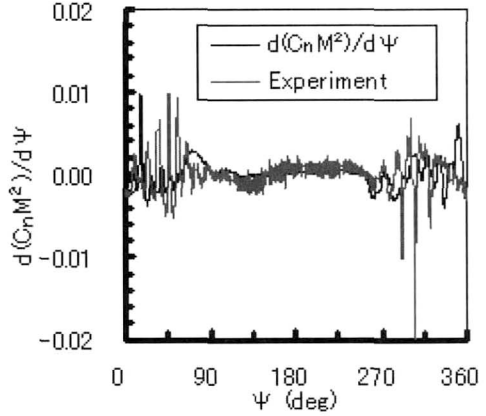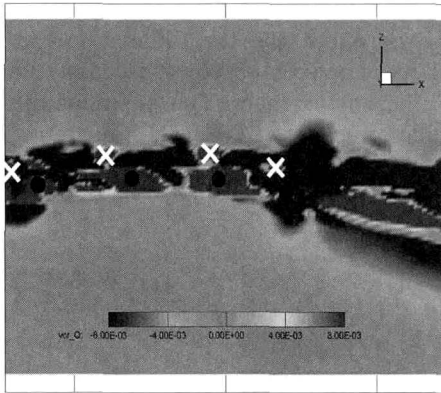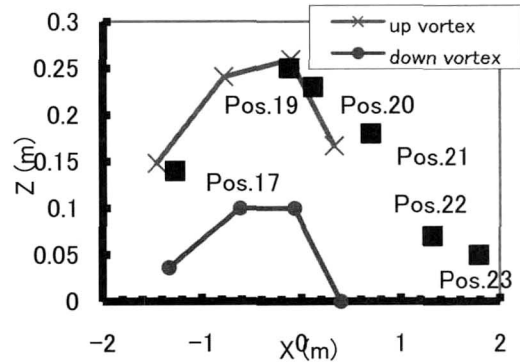Fig. 18. Calculated blade airload C_nM^2 plotted with HART II experimental result: (Position = 0.87m) (0° ~360°)

Fig. 19. Calculated blade airload derivative $d(C_nM^2)/d\Psi$ plotted with HART II experimental result: (Position = 0.87m) (0° ~360°)
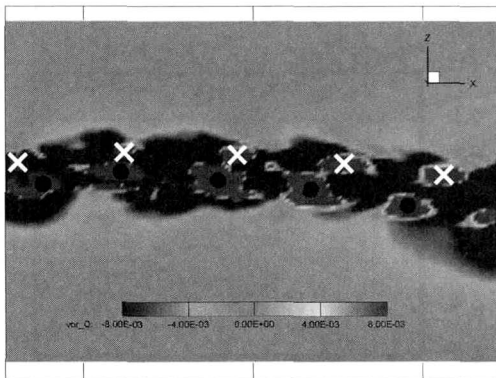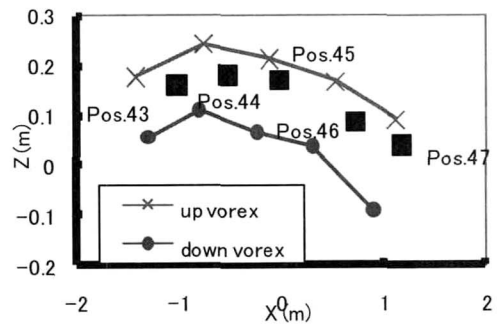

(a) Cross−Section (× and ● is vortex center)

(b) Comparison of calculated vortex center position and experimental results

Fig. 20. Position Y=1.4(m) (Advancing side)

(a) Cross−Section (× and ● is vortex center)

(b) Comparison of calculated vortex center position and experimental results

Fig. 21. Position Y=−1.4(m) (Rerating side)

For the first position corresponding to the creation of the vortex, the instantaneous data are rather well concentrated around the vortex center (about point 19 and 45). Then, when the age of the vortices grows, the locations of the vortex centers are more scattered. Such dispersion dose not only reflect the unsteadiness of the vortex, but also the uncertainty of the evaluation of the vortex center based on the location of extream values of vorticity or inner back ground mesh size.

Concluding Remarks

In this study, numerical capturing of the 2D and 3D blade—vortex interaction (BVI) are performed. From the results, we conclude as follows:

Conclusions for 2D BVI event:
1. As the incident angle is increased, the peak position of the BVI level shifts to the negative side.
2. The position shift is caused by the upwash ahead of an airfoil with incidence angle. The vortex moves upward while convected downstream in such a flowfield. So most important factor is the instant miss—distance when the vortex reaches at airfoil nose.

Conclusions for 3D BVI event:
1. The calculated blade airload C_nM^2 and its derivative $d(C_nM^2)/D\phi$ still deviate largely from the experiment with current grid resolutions.
2. The vortex location at advancing side (Y=1.4) and retreating side (Y=−1.4) show good agreement between the HART II experiment and the calculation.
3. Using finer inner back ground mesh and including elastic deformation to 3D BVI event are regarded as future task for better results.

References

1. J. Bailly, Y. Delrieux, P. Beaumier, "HART II: Experimental Analysis and Validation of ONERA Methodology for the Prediction of Blade—Vortex Interaction", 30th European Rotorcraft Forum, Mareille (France), September 2004.

2. G. Perez and J. Bailly, "USING HART II DATA BASE TO IMPROVE BVI NOISE PREDICTION," 32th European Rotorcraft Forum, Maastricht (Netherlands), September 2006.

3. C. Kitaplioglu, F.X. Caradonna, and M. McClur, "An Experimental Study of Parallel Blade—Vortex Interaction Aerodynamics and Acoustics Utilizing and Independently Generated Vortex", NASA/TM—1999—208790, July (1999).

4. C. Kitaplioglu, F.X. Caradonna, and C.L. Burley, "Parallel Blade—Vortex Interactions: An Experimental Study and Comparison with Computations", Journal of the American Helicopter Society, pp.272—281, July (1997).

5. Y. Inada, C. Yang, N. Iwanaga and T. Aoyama, "Efficient Prediction of BVI Noise Using Euler Solver with Wake Model," ROTOR KOREA 2007, October (2007).

6. S. Peron, C. Benoit, T. Renaud, J. Sides, Y. Tanabe, S. Saito, C. Yang, T. Aoyama, "ONERA/JAXA common investigations on CFD tools for an accurate prediction of BVI" ROTOR KOREA 2007, October (2007).

7. Y. Tanabe, S. Saito, C. Yang, and T. Aoyama, C. Benoit, J.−O. Gretay, G. Jeanfaivre, S. Peron, J. Sides, "Inviscid Numerical Simulations of 2D Parallel Blade—Vortex Interaction," JAXA−RR−06−042E, also ONERA Technical Report, No. RT 1/11474 DSNA, March 2007.

8. Y. Tanabe, S. Saito, K. Takasaki and H. Fujita, "A Parametric Study on Parallel Blade—Vortex Interaction for Helicopter Rotor," JAXA−RR−07−051E, February 2008

9. A. Ochi, T. Aoyama, S. Saito, E. Shima and E. Yamakawa, "BVI Noise Predictions by Moving Overlapped Grid Method," 55th American Helicopter Society Annual Forum, May (1999).

10. E. Shima and T. Jounouchi, "Role of CFD in Aeronautical Engineering (No.14) □ AUSM Type Upwind Schemes − ", NAL SP−34, 7−12, (1999).

11. Jameson and T.J. Baker, "Solution of Euler Equations for Complex Configuration, " AIAA Paper 83−1929 (1983).

12. H.C. Yee, and A. Harten, "Implicit TVD Schemes for Hyperbolic Conservation Laws in Curvilinear Coordinates," AIAA Journal, 25(2), 266−274, (1987).